*Articles*

# PA1b, an Insecticidal Protein Extracted from Pea Seeds (*Pisum sativum*): $^1$H-2-D NMR Study and Molecular Modeling[†,‡]

Laurence Jouvensal,*[,§] Laurence Quillien,[||] Eric Ferrasson,[||] Yvan Rahbé,[⊥] Jacques Guéguen,[||] and Françoise Vovelle[§]

*Centre de Biophysique Moléculaire, CNRS, Affiliated to Orleans University, Rue Charles Sadron, 45071 Orléans Cedex 2, France, UMR 0203 INRA/INSA de Lyon, BF2I (Biologie Fonctionnelle, Insectes et Interactions), Bâtiment Louis Pasteur, 20, Avenue Albert Einstein, 69621 Villeurbanne Cedex, France, and Unité de Recherche sur les Protéines Végétales et leurs Interactions, INRA, BP 71627, Rue de la Géraudière, 44316 Nantes Cedex 3, France*

*Received May 15, 2003; Revised Manuscript Received August 7, 2003*

ABSTRACT: PA1b (pea albumin 1, subunit b) is a 37-amino acid cysteine-rich plant defense protein isolated from pea seeds (*Pisum sativum*). It induces short-term mortality in several pests, among which the cereal weevils *Sitophilus* sp. (*Sitophilus oryzae*, *Sitophilus granarius*, and *Sitophilus zeamais*) that are a major nuisance for stored cereals, all over the world. As such, PA1b is the first genuine protein phytotoxin specifically toxic to insects, which makes it a promising tool for seed weevil damage control. We have determined the 3-D solution structure of PA1b, using 2-D homonuclear proton NMR methods and molecular modeling. The primary sequence of the protein does not share similarities with other known toxins. It includes six cysteines forming three disulfide bridges. However, because of PA1b resistance to protease cleavage, conventional methods failed to establish the connectivity pattern. Our first attempts to assign the disulfide network from NOE data alone remained unsuccessful due to the tight packing of the cysteine residues within the core of the molecule. Yet, the use of ambiguous disulfide restraints within ARIA allowed us to establish that PA1b belongs to the inhibitor cystine-knot family. It exhibits the structural features that are characteristic of the knottin fold, namely, a triple-stranded antiparallel $\beta$-sheet with a long flexible loop connecting the first to the second strand and a series of turns. A comparison of the structural properties of PA1b with that of structurally related proteins adopting a knottin fold and exhibiting a diverse range of biological activities shows that the electrostatic and lipophilic potentials at the surface of PA1b are very close to those found for the spider toxin ACTX-Hi:OB4219, thereby suggesting activity on ion channels.

The cereal weevils *Sitophilus* sp. (*Sitophilus oryzae*, *Sitophilus granarius*, and *Sitophilus zeamais*) are responsible for severe nuisance to stored cereals: every year, worldwide losses due to weevil attacks represent about 20% of the stocks. Plant pests can be controlled by chemical insecticides or by physical techniques (thermal or mechanical treatments or radiations). There are drawbacks, however: pesticides are damaging for human health as well as for the environment, and physical techniques are costly and sometimes difficult to handle. Recently, the technology of insect-resistant (transgenic) plants has emerged to circumvent crop pests and is now expanding very rapidly. Current research in this area focuses particularly on crystal proteins from the bacterium *Bacillus thuringiensis* (*1*) and on proteins from higher organisms, lectins, or enzyme inhibitors acting on key insects' digestive hydrolases (for reviews, see refs *2* and *3*). However, to date, these molecules have not proved efficient against the cereal weevils *Sitophilus* sp. either in artificial bioassays or *in planta* (*4*). The only transgene with a validated effect on stored product pests is currently the vitamin sequestrant avidin (*5*) of animal origin. All plants possess a certain degree of resistance toward insects, which is reflected in the limited number of insects capable of feeding on a given plant. This resistance, acquired during evolution, relies on several mechanisms involving the production of defense compounds, either proteic or not (*1*). Hence, the recent discovery of a protein extracted from pea and specifically toxic for cereal weevils has enlarged the potential for grain protection (*6*).

This protein, pea albumin 1b (PA1b),[1] extracted from pea seeds (*Pisum sativum*) includes 37 residues. It is the first genuine protein phytotoxin with an acute and specific *per os* toxicity on insects, which makes it an attractive candidate for the protection of crops against seed weevil damage. Several nucleotidic sequences coding for PA1b homologues

[†] E.F. was supported by the Agence Nationale de la Valorisation de la Recherche (ANVAR): Contract A9708331V/AT.

[‡] Swiss-Prot accession number: P08687. The ensemble of 15 NMR models has been deposited under PDB accession code 1P8B.

* To whom correspondence should be addressed. Phone: +33 (0)2 38 25 76 60. Fax: +33 (0)2 38 63 15 17. E-mail: jouvensa@cnrs-orleans.fr.

[§] Centre de Biophysique Moléculaire.

[||] Unité de Recherche sur les Protéines Végétales et leurs Interactions.

[⊥] UMR 0203 INRA/INSA de Lyon.

10.1021/bi034803l CCC: $25.00 
Published on Web 09/23/2003

have been characterized in pea (*7*), indicating the multigenic character of this novel toxin family in this species, and several PA1b-like peptides have also been characterized from other plants of the *Fabaceae* family (*8*, *9*). On the basis of the natural variability of the protein sequences and biological activities, an approach of directed mutagenesis is in progress to understand the structural features responsible for the entomotoxic properties of this new toxin family.

In this paper, we report on the determination of the 3-D solution structure of PA1b, using proton 2-D NMR spectroscopy and molecular modeling. The sequence of the protein does not share obvious similarities with other known toxins and includes six cysteines forming three disulfide bridges. However, owing to a resistance to protease cleavage, conventional methods for establishing the connectivity pattern have proved to be ineffective. The tight packing of the cysteine residues within the core of the molecule impeded our previous attempts to assign the disulfide network from NOE data. Recently, the use of ambiguous disulfide restraints within ARIA allowed us to establish that PA1b belongs to the inhibitor cystine-knot family (ICK). It exhibits all the structural features characteristic of the knottin fold, namely, a triple-stranded antiparallel $\beta$-sheet with a long flexible loop connecting the first to the second strand and a series of turns. This solution structure is compared to that of other structurally related proteins with a view to inferring hypotheses about the PA1b mode of action. Common features with the toxin ACTX-Hi:OB4219 from the insectivorous spider *Hadronyche infensa* are pointed out.

## MATERIALS AND METHODS

*NMR Sample Preparation.* Albumins were extracted from winter pea seeds (cv. Frilène) at a pilot scale (*10*). The albumins soluble in 60% methanol were loaded on an anion exchange column (DEAE Sepharose Fast Flow). PA1b has been purified from the nonretained chromatography fraction by RP-HPLC (Si-C18) as described previously (*6*). A total of 4.7 mg of purified PA1b have been solubilized in 600 $\mu$L of a mixture of TFE and $H_2O$ in a 1:1 ratio (v/v), 0.02% $NaN_3$, leading to a protein concentration of 2.1 mM. The final pH of the PA1b solution, adjusted with minute increments of 1 N HCl, was 4.8. The amide protons exchange rate was determined after lyophilization of this sample and dissolution in TFE-$d_3$/$D_2O$.

*NMR Experiments.* All $^1$H NMR spectra were recorded on a 600 MHz VARIAN INOVA spectrometer equipped with a *z*-axis field-gradient unit. Data were processed using NMRPipe/NMRDraw (*11*). NOESY (*12*), clean-TOCSY (*13*), and DQF-COSY (*14*) experiments were performed at two different temperatures to solve assignment ambiguities (285 and 293 K). Water suppression was achieved using presaturation during the relaxation delay (1.5 s) and, in the case of NOESY experiments, during the mixing time. NOESY spectra were acquired using mixing times of 120 and 300 ms; clean-TOCSY was performed with a mixing time of 80 ms. All spectra were referenced to the residual $H_2O$ signal set as the carrier frequency, 4.897 ppm at 285 K and 4.821 ppm at 293 K. Amide deuterium/proton exchange ratios were monitored by recording 1-D and short NOESY spectra at different times over the 26 h following the dilution of the protein in a deuterated solution. The amide protons that were not exchanged 24 h after dilution were identified as slowly exchanging protons and interpreted either as hydrogen-bond donors or as protons not accessible to the solvent. The identification of amino acid spin systems and the sequential assignment were done using the standard strategy described by Wüthrich, applied within a graphical software, XEASY (*15*).

*Structure Calculations.* Distance constraints were determined by volume integration of correlations observed in the NOESY spectrum recorded at 293 K with a mixing time of 120 ms, using the XEASY software. 15 $\phi$ torsion angle restraints resulted from $^3J_{NH-H\alpha}$ coupling constants estimated from the NOESY spectrum using the INFIT program (*16*). These $\phi$ angles were restrained within the range $-60 \pm 30°$ for $^3J_{NH-H\alpha} < 5$ Hz; $-60 \pm 40°$ for $5 \leq {}^3J_{NH-H\alpha} \leq 6$ Hz; $-120 \pm 30°$ for $8 \leq {}^3J_{NH-H\alpha} \leq 9$ Hz; and $-120 \pm 20°$ for $^3J_{NH-H\alpha} > 9$ Hz. Moreover, at the end of the calculations, seven hydrogen bond restraints were enforced between NH and C═O groups for pairs of residues involved in secondary structure elements when the amide proton was not completely exchanged with $D_2O$ after 24 h. For each hydrogen bond, the $H_N-O$ and $N-O$ lower limit restraints were set to 1.8 and 2.8 Å, respectively, and the upper limits to 2.2 and 3.2 Å.

The dihedral angles and distance restraints obtained from measured NMR parameters were used in structural calculations to determine the conformation of the peptide. Along with a table of chemical shifts, they were introduced as input to ARIA 1.1 (*17*) implemented in CNS 1.1 (*18*). ARIA calculations were initiated using default parameters. In the first instance, the disulfide bridges topology was established using distance restraints (from 0 to 2.1 Å) allowing ambiguous partnership between S atoms, combined with NMR-derived structural information. The lower $S-S$ distance limit was set to 0 to allow intermediate unphysical situations when more than two sulfur atoms are in close proximity. Moreover, the van der Waals radii of the Cys S$\gamma$ atoms were decreased to allow close contacts between atoms prone to form disulfide bonds. Subsequently, S$\gamma-$S$\gamma$ covalent bonds between the paired cysteines were included in the topology files. In the final ARIA run, the number of structures generated in the seventh and eighth iterations was increased to 40 and 100, and after refinement by molecular dynamics simulation in water, the 15 lowest energy structures were used for statistical analysis.

The structures were displayed and analyzed using the MOLMOL (*19*) and SYBYL (TRIPOS Inc., St. Louis, MO) programs, and their quality was evaluated using the PROCHECK (*20*) and PROMOTIF (*21*) softwares. Formation of hydrogen bonds was established according to distance criteria. Lipophilic and electrostatic potentials were calculated and represented using the MOLCAD option (*22*) of SYBYL.

[1] Abbreviations: PA1b, pea albumin 1; PAFP-S, Pokeweed antifungal peptide from seeds (from *Phytolacca americana*); ACTX-Hi: OB4219, atracotoxin from the Australian funnel-web spider *Hadronyche infensa* (Orchid Beach); ICK, inhibitor cystine-knot; RP-HPLC, reverse-phase high-pressure liquid chromatography; TFE, trifluoroethanol; 3-D, three-dimensional; $^1$H, proton; 2-D NMR, two-dimensional nuclear magnetic resonance; DQF-COSY, double quantum filtered correlation spectroscopy; NOE, nuclear Overhauser effect; NOESY, NOE spectroscopy; TOCSY, total correlation spectroscopy; RMSD, root-mean-square deviation.

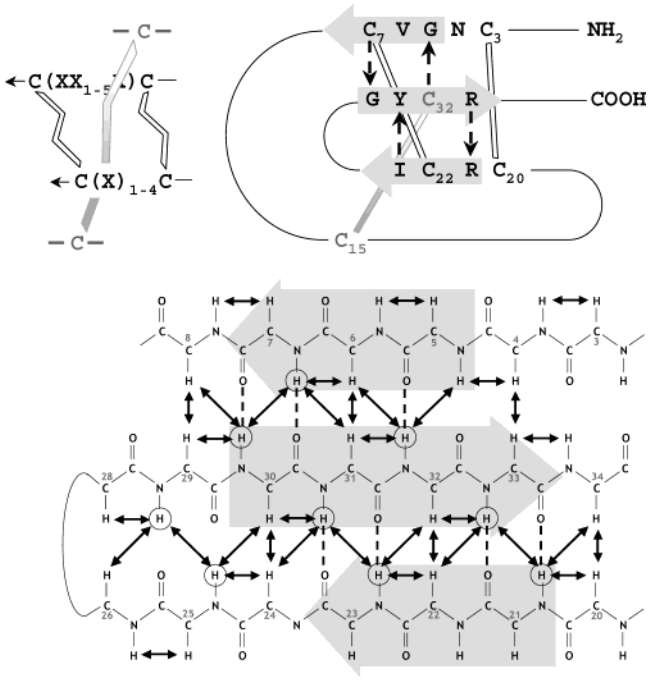


FIGURE 1: (Top) Consensus motif for inhibitor cystine-knots as defined by Pallaghy et al. (*61*) and Craik et al. (*30*) identified in PA1b structure: the $\beta$-strands are represented as gray arrows with the consensus residues shown as one-letter symbols (X can be any residue). Hydrogen bonds in the cystine-knot motif are shown as dashed arrows from the amide proton to the carbonyl. (Bottom) Schematic diagram of the triple-stranded antiparallel $\beta$-sheet structure of PA1b deduced from analysis of the NMR data: observed backbone interstrand NOEs are indicated as arrows; slowly exchanging amide protons are circled; and hydrogen bonds are indicated as dashed lines.

## RESULTS

*NMR Data*. PA1b was extracted from pea seeds (*P. sativum*) as described in the Materials and Methods. Sequence specific assignments were performed according to standard procedures (*23*) allowing complete resonance assignment of all backbone protons and of most side-chain protons (see Supporting Information for the chemical shift table).

Low-field shifted Hα chemical shifts, large $^3J_{NH-H\alpha}$, slowly exchanging amide protons, and a characteristic set of interstrand Hα($i$)−Hα($j$), NH($i$)−NH($j$), and Hα($i$)−NH($j$) connectivities delineate a triple-stranded $\beta$-sheet (Figure 1). The presence of several medium range NOEs in the remainder of the sequence suggests that it consists mainly of loops and turns.

Strong sequential Hα−H$\delta$ NOE cross-peaks for Xxx-Pro confirm trans peptide bonds for Pro9, Pro14, Pro24, and Pro35, while a strong sequential Hα−Hα cross-peak between Met12 and Pro13 indicates the presence of a cis bond. The Met12−Pro13 peptide bond was thus forced to adopt a cis configuration.

*Identification of the Disulfide Bonds.* PA1b contains six disulfide-linked cysteine residues as indicated by mass analysis. However, the disulfide connectivities were unknown due to the resistance of the protein to enzymatic degradation. Attempts to identify disulfide bridges from Hα−H$\beta$ and H$\beta$−H$\beta$ NOE contacts observed between the cysteines involved in the linkage were unsuccessful due to frequent cross-peak overlaps involving cysteine protons and did not permit us to reach a clear-cut conclusion. For a protein containing six cysteines, there are 15 theoretically possible ways of connecting them by pairs. Two different approaches were used to establish whether the NOE data were sufficient to infer a single compatible connectivity pattern. In the first approach, a family of structures was calculated on the basis of the NOE constraints, without any assumption on the disulfide connectivities. In the second one, sets of structures were calculated for each of the 15 possible disulfide arrangements. In both approaches, the structures were obtained from manually attributed NOE data, using a torsion angle simulated annealing method within DYANA (*24*) followed by energy minimization within XPLOR (*25*). At this time, the spatial proximity of the six cysteine residues within the core of the molecule did not allow the unequivocal assignment of the cystine bonding pattern on the basis of the NMR-restraints set used since neither energetical nor stereochemical criteria allowed us to decide in favor of one among the following possibilities: cystine-knot pairing, Cys(I−IV), Cys(II−V), and Cys(III−VI); thionin-like pairing: Cys(I−VI), Cys(II−V), and Cys(III−IV); and other, Cys(I−IV), Cys(II−VI), and Cys(III−V).

Therefore, an alternative approach was used to identify the disulfide connectivities, based on the concept of ambiguous distance restraints initially introduced by Nilges (*26*) and now currently used in ARIA (*17*). The unknown disulfide connectivities were introduced in a two-stages protocol (*27*, *28*) as ambiguous constraints between one specific Cys S$\gamma$ atom and all other Cys S$\gamma$ atoms; the SUM option (*26*) was used for averaging. Starting from a set of 631 NOE constraints manually assigned, mostly intraresidue and sequential as well as unequivocal long-range NOEs, the global fold of the protein was first determined starting from randomized coordinates. At this stage, only the NMR data were used, without any constraint on sulfur atoms. A large number of additional NOEs were assigned automatically and incorporated into the restraint data set during the iterative calculations of ARIA. Last, in the final run, 150 structures with the lowest experimental energy were selected from the total of 300 conformers obtained at the end of iteration 7 and used as starting coordinates for the last iteration in which ambiguous intersulfur restraints were added. To establish the structural statistics for the disulfide pairing, 43 structures with nonphysical topologies containing more than three disulfide bridges were rejected from the structure ensemble. Among the remaining 107 structures, 95% adopt the knottin pairing and only 5% the thionin-like pairing. The correct disulfide pairing is therefore Cys(I−IV), Cys(II−V), and Cys(III−VI), in agreement with the consensus sequence $CX_{3-7}CX_{3-8}CX_{0-7}CX_{1-4}CX_{4-13}C$ found for polypeptides from diverse sources adopting the inhibitor cystine-knot motif (*29*, *30*).

*Structure Calculations.* In a subsequent ARIA run, the S$\gamma$−S$\gamma$ covalent bonds were included between the paired cysteines. After eight iterations, the structures were refined by molecular dynamics in an explicit solvent environment (*31*) using a data set comprising 858 distance restraints, with an average of 23 restraints per residue (Table 1). In addition, 15 dihedral angle restraints were deduced from the $^3J_{NH-H\alpha}$ coupling constants, and seven restraints were added to account for main chain hydrogen bonds. Finally, 15 structures in very good agreement with all the experimental data and

Table 1: Structural Statistics for the Final 15 Models of PA1b

| | |
|---|---|
| **Conformational Restraints** | |
| NOE based distance bonds | |
| unambiguous restraints | 851 |
| intraresidue ($\|i-j\|=0$) | 354 |
| sequential ($\|i-j\|=1$) | 221 |
| medium range ($2 \le \|i-j\| \le 4$) | 79 |
| long range ($\|i-j\| \ge 5$) | 197 |
| ambiguous restraints[a] | 7 |
| dihedral angle restraints | 15 |
| hydrogen bonds | 7 |
| **Restraint Violations (Number per Structure)** | |
| distance restraints >0.3 Å | 0 |
| dihedral angle restraints >5° | 0 |
| **RMS Deviation from Standard Geometry** | |
| bond length (Å) | 0.0040 ± 0.0002 |
| bond angles (deg) | 0.4796 ± 0.0225 |
| impropers (deg) | 0.4129 ± 0.0440 |
| **RMS Deviation from the Experimental Restraints** | |
| NOEs (Å) | 0.0174 ± 0.0018 |
| dihedral restraints (deg) | 1.01 ± 0.23 |
| **Ramachandran plot (%)[b]** | |
| most favored regions | 77.7 |
| additional allowed regions | 20.8 |
| generously allowed regions | 0.5 |
| disallowed regions | 1 |
| **Energies (kcal mol$^{-1}$)** | |
| electrostatic | −1082.3 ± 42.7 |
| van der Waals | −100.0 ± 8.6 |
| $E_{NOE}$ | 13.4 ± 2.8 |
| $E_{CDIH}$ | 1.0 ± 0.5 |
| total energy | −995.2 ± 47.5 |

Average RMSD (pairwise, Å)[c]

| | bb (N−Cα−C′) | all heavy atoms |
|---|---|---|
| whole (2−36) | 0.73 ± 0.17 | 1.23 ± 0.15 |
| secondary structures (4−7, 13−17, 21−23, 30−33) | 0.54 ± 0.13 | 1.13 ± 0.18 |
| triple-stranded β-sheet (4−7, 21−23, 30−33) | 0.28 ± 0.09 | 1.07 ± 0.22 |
| $3_{10}$ helix (13−17) | 0.48 ± 0.21 | 0.87 ± 0.31 |
| hairpin loop (24−29) | 0.21 ± 0.11 | 0.37 ± 0.16 |
| loop (8−20) | 0.63 ± 0.16 | 1.20 ± 0.22 |

[a] Ambiguous distance restraints contain contribution from distances between all pairs of protons that are possible assignments of the NOE. [b] Determined by PROCHECK. [c] Calculated using MOLMOL.

the standard covalent geometry (Table 1) were selected for further analysis. For these structures, no experimental distance constraint violation greater than 0.3 Å is observed, nor is any torsion angle violation greater than 5°, and the root-mean-square deviations (RMSD) with respect to the standard geometry are low. Both negative van der Waals and electrostatic energy terms are indicative of favorable nonbonded interactions. Moreover, the Ramachandran plot exhibits 98.5% of the ($\phi$, $\psi$) angles of the 15 converged structures in the most favored regions and additional allowed regions according to the PROCHECK software nomenclature.

*Structure Description.* The overall fold of PA1b is formed by a triple-stranded antiparallel β-sheet with a topology of (+2*x*, −1), consisting of strand 1 (Asn4-Cys7) hydrogen bonded to strand 3 (Gly30-Arg33), which in turn is hydrogen bonded to strand 2 (Arg21-Ile23). Figure 1 shows a schematic diagram of the β-sheet structure, including the observed regular backbone NOEs and hydrogen bonds. Except between Gly5 and Cys32 where only the C═O (5)−NH (32) hydrogen bond is observed, most canonical hydrogen bonds are formed and are confirmed by the $^1$H-$^2$H exchange experiments. A long loop L1 (Ser8-Cys20) connects strand 1 to strand 2. All 15 structures exhibit a type I β-turn between Ser8 and Glu11, followed by a type VIb β-turn between Glu11 and Pro14, and in 10 out of the 15 selected structures, a $3_{10}$ helix turn is found by PROMOTIF between residues Pro13 and Thr17, allowing the formation of the Cys(15)−Cys(32) disulfide bridge. The L1 loop is linked to the second strand of the β-sheet by another β-turn (Thr17-Cys20). The second and third strands are linked by a hairpin loop L2 including a series of turns: a reverse γ-turn between Ile23 and Val25, stabilized by the canonical C═O (23)−NH (25) hydrogen bond found on the 15 selected structures, followed by a β-turn between Gly26 and Ile29. In this case, the canonical *i*, *i* + 3 hydrogen bond is not formed, replaced by a NH (26)−C═O (29) hydrogen bond formed on seven out of the 15 selected structures. The structure is further stabilized by the three disulfide bridges of the cystine-knot motif. The first one links the beginning of strand 1 to the beginning of strand 2; the second one links the end of strand 1 to strand 2, thus connecting these two parallel but nonadjacent strands; and the last one goes through the ring, linking the $3_{10}$ helix turn to strand 3 (Figure 2A).

As evidenced by the structural statistics (Table 1) and by a sausage representation of the backbone for the selected structures (Figure 2B), the structure of PA1b is well-defined. The pairwise RMS deviations on the N, Cα, and C′ backbone atoms of residues 2−36 are 0.73 Å and drop to 0.28 Å when calculated on the secondary structure elements. The largest variability is found for loop L1, where the RMS deviations on the backbone atoms are 0.63 Å.

Because of the presence of numerous NOEs, several side chains adopt a single conformation. In particular, significantly low circular variances (*32*) for $\chi_1$ and $\chi_2$ angles are observed for the hydrophobic and aromatic residues. In contrast, the side chains of the hydrophilic residues display large conformational variability, except for Arg21, which is extremely well-defined.

## DISCUSSION

We have determined the 3-D solution structure of PA1b, a protein from pea seeds active against cereal weevils. The use of ambiguous intersulfur restraints within ARIA allowed us to assign the disulfide connectivities of the six cysteines. The structure of PA1b displays all the characteristics of the inhibitor cystine-knot fold, including a triple-stranded antiparallel β-sheet and the cystine-knot motif of disulfide bridges. This structural motif, initially reported for trypsin inhibitors from cucurbits (*33*, *34*), is also found for a variety of proteins from plants, fungi, crabs, cone snails, and spiders, exhibiting various biological activities. They include $K^+$ channel blockers (κ-conotoxin (*35*), HpTX2 (*36*)); $Ca^{2+}$ channel blockers (ω-agatoxins (*37*−*40*), ω-conotoxins (*41*)); $Na^+$ channel blockers (δ-atracotoxins (*42*)); trypsin and α-amylase inhibitors (*43*, *44*); antimicrobial peptides (*45*, *46*); and peptides with sweet-taste suppressing effects (*47*). In addition, a series of macrocyclic peptides from plants with diverse biological activities but unknown functions in plants (*30*), such as kalata B1 (*48*), also display a knottin fold.

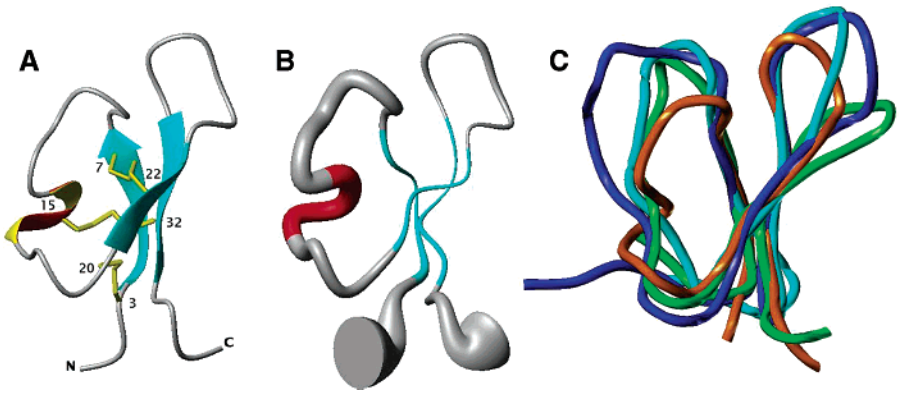


FIGURE 2: (A) Ribbon representation of PA1b lowest energy structure. (B) Sausage representation of 15 structures of PA1b. The radius of the sausage is proportional to the average displacement of the Cα atoms to the mean structure. (C) Superposition of the backbones of PA1b (orange), PAFP-S (cyan), tachystatin A (blue), and ACTX-Hi:OB4219 (green), fitted on the secondary structure elements according to Table 2.

Table 2: Structural Alignment of PA1b with Other Inhibitor Cystine-Knot Proteins

| | * * --- * * | RMS[a] | $N_{ali}$[b] |
|---|---|---|---|
| Pa1b | ASCNGVCSPFEMPP---CGTSACRCIPV-G-LVIGYCRNPSG | | |
| PAFP-S | AGCIKNGGRCNASAGPPY-CC--S-SYCFQIAG-QSYGVCKNR-- | 0.81 Å | 16 |
| Pa1b | ASCNGVCSPFEMPP---CGTSACRCIPV-GL-VIGYCRNPSG | | |
| Tachystatin A | YSRCQLQGFNCVVRSYGLPTIPCCRGLTCRSYFPGSTYGRCQRY-- | 0.90 Å | 17 |
| Pa1b | ASCNGVCSPFEMPP---CGTSACRCIPVG--LVIGYCRNPSG | | |
| ACTX-Hi:OB4219 | KCLAEAADCSPWSGDS--CC--KPYLCSCIF-FYP-CSCRPKGW | 0.90 Å | 15 |

[a] RMS deviation calculated over aligned residues. [b] Number of aligned residues.

Despite variations in the number of amino acids between the successive half cystines (*49*), the structures of all these proteins display a I−IV, II−V, and III−VI disulfide array with Cys(III−VI) passing through the ring formed by the other disulfide bridges and their connecting backbone segments.

As already observed for other cysteine-rich proteins with a different fold, such as plant and insect defensins or scorpion toxins, all adopting a CSα$\beta$ motif (*50*), the protein fold with its specific arrangement of disulfide bridges confers a high stability to the structure but is not a determining factor for the function specificity (*51*). As far as we know, except possibly for kalata B1, which shows inhibitory effects on the growth and development of larvae from the lepidopteran species *Helicoverpa punctigera* (*52*), PA1b is the first plant protein causing acute insect toxicity and adopting a knottin fold reported so far. The cystine-knot appears to confer a remarkably high degree of stability since PA1b is resistant to digestion by trypsin, and its biological activity is preserved when heated at 120 °C for 15 min (B. Delobel, personal communication). The 3-D structure of PA1b is extremely compact; most sulfur atoms are in close contact. Furthermore, this tight packing of the cystine residues is likely to explain the resistance of PA1b to enzymatic degradation and also our difficulties in determining the disulfide array.

The mode of action of PA1b on cereal weevils is still unclear: a high affinity binding site for PA1b has been characterized in *Sitophilus* extracts, but this binding site has not yet been purified, and the exact mechanism of toxicity remains unknown (*53*). However, PA1b does not show any enzymatic or enzyme inhibiting activity (*54*). Therefore, engineering of the natural pea toxin to design more potent molecules, or molecules active on resistant weevil strains, relies on sequence comparisons with PA1b-like molecules of the *Fabaceae* family and also on a detailed comparison of the 3-D structure of PA1b with structurally related proteins. For this purpose, we searched for structural neighbors using TOP (*55*), DALI (*56*), and SSM.[2] The search led to a large number of proteins including knottins but also mammalian defensins, antifungal plant and insect defensins, and scorpion toxins. The 3-D structures of these proteins contain three-stranded antiparallel $\beta$-sheets, but they exhibit different disulfide arrays. Therefore, only structural neighbors adopting a knottin fold were taken into consideration, even if the alignment scores were not the best. These structural neighbors are ACTX-Hi:OB4219, a toxin from the Australian spider *Hadronyche infensa* ((*57*); PDB code 1kqh); tachystatin A, an antimicrobial protein from the Japanese horse shoe crab *Tachypleus tridentus* (ref *46*; PDB code 1cix); and PAFP-S, an antifungal protein from the seeds of *Phytolacca americana* (ref *45*; PDB code 1dkc).

The best-fit superposition of the protein structures is obtained for the backbone atoms of residues in the three $\beta$-strands or lining these $\beta$-strands (Figure 2C). Loops L1

[2] SSM: EBI service for protein alignment and comparison in 3-D, authored by E. Krissinel and K. Henrick, publicly available at http://www.ebi.ac.uk/msd-srv/ssm.

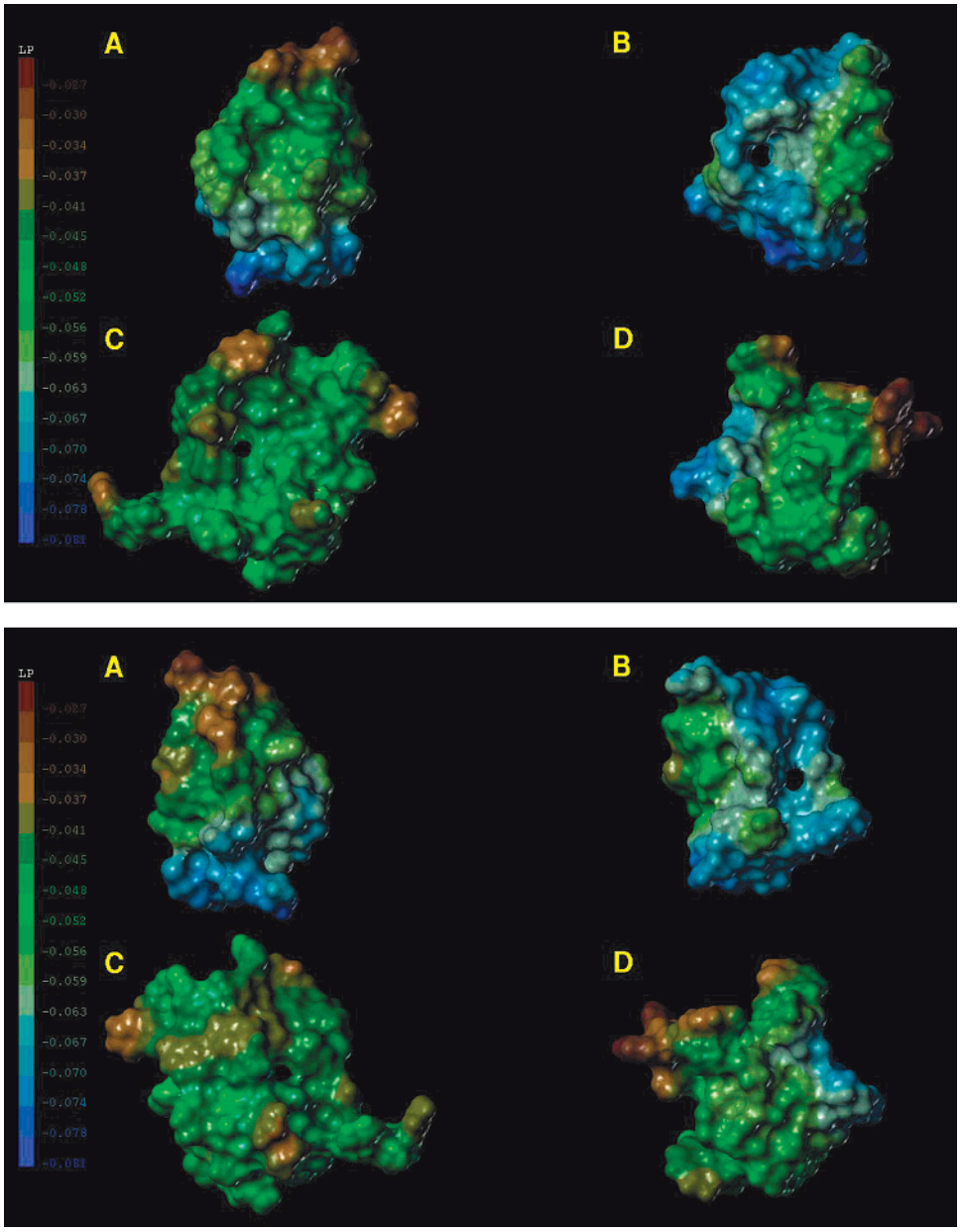


FIGURE 3: Lipophilic potentials calculated with the MOLCAD option of SYBYL at the Connolly surfaces of (A) PA1b, (B) PAFP-S, (C) tachystatin A, and (D) ACTX-Hi:OB4219 in the same orientation as in Figure 2C, using a common hydrophobic scale. Hydrophobic and hydrophilic areas are displayed in brown and blue, respectively. Green surfaces represent an intermediate hydrophobicity. A 180° rotation with respect to a vertical axis is applied from the upper to the lower panel.

and L2 have very different lengths and adopt very different conformations from one molecule to the other, leading to a poor superposition. The RMS deviations on the backbone atoms of the structurally aligned residues range between 0.81 Å (PAFP-S) and 0.90 Å (OB4219 and tachystatin) for a number of aligned residues varying between 15 (PA1b and OB4219) and 17 (PA1b and tachystatin) (Table 2). These numbers are not significantly different considering the variability of the NMR structures of the proteins. A comparison of the sequences of the structurally aligned residues shows that there are very few sequence similarities. It can also be noted that, due to the varying number of residues between the cysteines in the different sequences, only the three cysteines Cys7, Cys22, and Cys32 (PA1b numbering) are structurally aligned, which means that the II−V disulfide bridge is well-preserved among the selected structures.

To extend our comparisons, we have calculated the electrostatic and lipophilic potentials at the Connolly surfaces of the proteins. These molecular properties can be derived from the 3-D structures and are related to the functions of the proteins. The distribution of the hydrophobic potentials calculated with MOLCAD at the surface of PA1b is characteristic of an amphipathic structure (Figure 3A). There is clearly a hydrophobic face formed by the residues of the hydrophobic loop L2: Val25, Leu27, Val28, and Ile29 but also by the facing residue Phe10 of L1. The hydrophilic face, situated at the other pole of the molecule including the N- and C-termini and a part of L1, arises from polar residues: Ser2, Asn4, Thr17, Ser18, Asn34, and Ser36. Due to the proximity of the hydrophobic residues Phe10 and Met12, the charged residue Glu11 is in an intermediate environment. The two facing arginines (Arg21 and Arg33) on strands 2

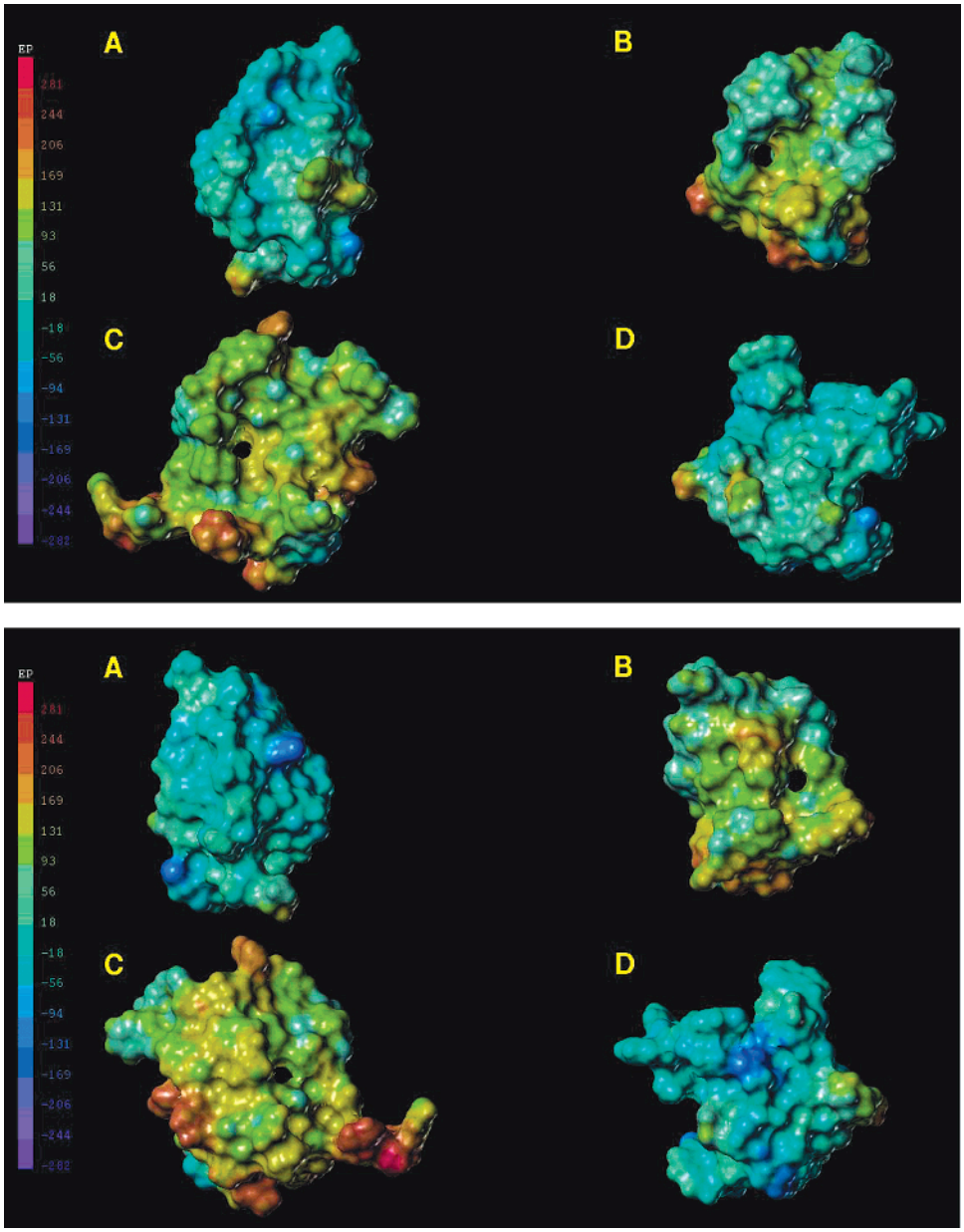


FIGURE 4: Electrostatic potentials at the Connolly surfaces of (A) PA1b, (B) PAFP-S, (C) tachystatin A, and (D) ACTX-Hi:OB4219 in the same orientation as in Figure 2C, using a common electrostatic scale. Positive and negative areas are displayed in red and blue, respectively. Cyan surfaces represent neutral areas. A 180° rotation with respect to a vertical axis is applied from the upper to the lower panel.

and 3 adopt a similar orientation with respect to the $\beta$-sheet and also lie in an intermediate environment, just at the limit of the hydrophilic zone. When the hydrophobic potentials are calculated using the same hydrophobic scale, the surface of PAFP-S (Figure 3B) appears mainly hydrophilic, with a small hydrophobic spot due to Phe25, while the surface of tachystatin (Figure 3C) shows an intermediate hydrophobicity (green surface), with hydrophobic patches corresponding to the numerous aromatic residues: five tyrosines (1, 16, 32, 38, 44) and two phenylalanines (9, 33). The only molecule also showing an amphipatic surface is OB4219 (Figure 3D), with a hydrophobic pole situated at the same position as in PA1b and a hydrophilic one at the N-terminus. The amphipathy of the molecule is, however, less marked than for PA1b, and there is an additional hydrophobic spot corresponding to Trp12. This amphiphilic character of PA1b may favor its interaction with membranes.

Regarding the electrostatic properties, PA1b, with one negatively charged residue (Glu11) and two positively charged residues (Arg21 and Arg33), is rather neutral as illustrated by the representation of the electrostatic potentials at the surface of the molecule that range between −147 and 159 kcal mol$^{-1}$ (Figure 4A). The positive patches in brown correspond to the two arginines and to the N-terminus, while the negative ones in blue come from Glu11 and from the C-terminus. In contrast, the surfaces of PAFP-S and tachystatin are more cationic (Figure 4B,C). PAFP-S has four positively charged residues (two Arg and two Lys) and tachystatin six (six Arg). However, for these two molecules the charge distributions are rather different, leading to different patterns for the potentials: tachystatin is more cationic than PAFP-S, with potentials ranging from −71 to 281 kcal mol$^{-1}$ versus −74 to 213 kcal mol$^{-1}$ for tachystatin and PAFP-S, respectively. The distribution of electrostatic

potentials at the surface of OB4219 is rather similar to that found for PA1b, with an identical amplitude of variation (−145 to 167 kcal mol$^{-1}$) (Figure 4D). OB4219 has the same global charge as PA1b, but the number of charged residues is much larger: its sequence displays four positively charged residues (one Arg and three Lys) and three negatively charged (one Glu and two Asp). However, as for PA1b, these charged residues are rather scattered on the sequence, especially the negative charges, which explains the similarity in the distributions of potentials.

There is clearly no correlation between the surface distributions of hydrophobic and electrostatic potentials of PA1b and of the two antimicrobial proteins PAFP-S and tachystatin. PAFP-S is a purely antifungal protein, whereas tachystatin is active against fungi and various bacterial strains. Both are cationic molecules, like most antimicrobial proteins, while PA1b is a quite neutral molecule; furthermore, despite a marked amphipathy, comparable to that observed for antifungal insect defensins (*51*, *58*), which led us to suspect an antifungal activity, PA1b is not effective, at least on the few fungal strains tested (data not shown). In contrast, hydrophobic and electrostatic potentials at the surface of the spider toxin OB4219 are very close to those of PA1b. Despite the presence of an additional disulfide bridge, OB4219 is the only molecule of our panel showing some sequence similarities with PA1b in two regions that may be of special importance to the activity of PA1b. In particular, both molecules display a stretch of hydrophobic residues, located in loop L2, facing a hydrophobic residue of L1, Phe10 for PA1b, and Trp12 for OB4219. These residues are well-conserved among the homologues of PA1b members of the *Fabaceae* family, active on cereal weevils. Sequence analogies also appear in loop L1, in particular in the segment Cys-Ser-Pro-Phe-Glu (Table 2), which is also well-preserved among the members of the *Fabaceae* family (S. Louis, personal communication). So far, there is no clear evidence concerning the biological activity of OB4219. It is one of the major components of the venom from an insectivorous spider, and it shows structural analogies with $\mu$-agatoxins I and IV (*59*), two sodium channel inhibitors (*60*), indicating that the target of OB4219 is presumably a voltage-gated ion channel. It is rather puzzling to note that our entomotoxin PA1b shows structural analogies with a toxin from an insectivorous spider. This may be indicative of a common or neighboring mode of action, tentatively as an ion channel blocker. Such a hypothesis remains of course to be confirmed, but it is consistent with the inhibitory role found for all proteins of the knottin family whose mode of action is known.

## ACKNOWLEDGMENT

We thank A. Caille for her technical assistance and kind support in the acquisition and analysis of the NMR data.

## SUPPORTING INFORMATION AVAILABLE

One table containing $^1$H chemical shifts for PA1b. This material is available free of charge via the Internet at http://pubs.acs.org.

## REFERENCES

1. Schuler, T. H., Poppy, G. M., Kerry, B. R., and Denholm, I. (1998) Insect-resistant transgenic plants, *Trends Biotechnol. 16*, 168−175.
2. Franco, O. L., Rigden, D. J., Melo, F. R., and Grossi-De-Sa, M. F. (2002) Plant α-amylase inhibitors and their interaction with insect α-amylases, *Eur. J. Biochem. 269*, 397−412.
3. Carlini, C. R., and Grossi-de-Sa, M. F. (2002) Plant toxic proteins with insecticidal properties. A review on their potentialities as bioinsecticides, *Toxicon 40*, 1515−1539.
4. Pittendrigh, B. R., Huesing, J. E., Shade, R. E., and Murdock, L. L. (1997) Effects of lectins, Cry1A/Cry1B Bt δ-endotoxins, PAPA, protease and α-amylase inhibitors on the development of the rice weevil, *Sitophilus oryzae*, using an artificial seed bioassay, *Entomol. Exp. Appl. 82*, 201−211.
5. Kramer, K. J., Morgan, T. D., Throne, J. E., Dowell, F. E., Bailey, M., and Howard, J. A. (2000) Transgenic avidin maize is resistant to storage insect pests, *Nat. Biotechnol. 18*, 670−674.
6. Delobel, B., Grenier, A. M., Guéguen, J., Ferrasson, E., and Mbaiguinam, M. Utilisation d'un polypeptide dérivé d'une albumine PA1b de légumineuse comme insecticide, French Patent 98 05877, 1998.
7. Higgins, T. J. V., Chandler, P. M., Randall, P. J., Spencer, D., Beach, L. R., Blagrove, R. J., Kortt, A. A., and Inglis, A. S. (1986) Gene structure, protein structure, and regulation of the synthesis of a sulfur-rich protein in pea seeds, *J. Biol. Chem. 261*, 11124−11130.
8. Watanabe, Y., Barbashov, S. F., Komatsu, S., Hemmings, A. M., Miyagi, M., Tsunasawa, S., and Hirano, H. (1994) A peptide that stimulates phosphorylation of the plant insulin-binding protein. Isolation, primary structure and cDNA cloning, *Eur. J. Biochem. 224*, 167−172.
9. Ilgoutz, S. C., Knittel, N., Lin, J. M., Sterle, S., and Gayler, K. R. (1997) Transcription of genes for conglutin γ and a leginsulin-like protein in narrow-leafed lupin, *Plant Mol. Biol. 34*, 613−627.
10. Crevieu, I., Berot, S., and Gueguen, J. (1996) Large scale procedure for fractionation of albumins and globulins from pea seeds, *Nahrung 40*, 237−244.
11. Delaglio, F., Grzesiek, S., Vuister, G. W., Zhu, G., Pfeifer, J., and Bax, A. (1995) NMRPipe: a multidimensional spectral processing system based on UNIX pipes, *J. Biomol. NMR 6*, 277−293.
12. Kumar, A., Ernst, R. R., and Wüthrich, K. (1980) A 2-D nuclear Overhauser enhancement (2-D NOE) experiment for the elucidation of complete proton-proton cross-relaxation networks in biological macromolecules, *Biochem. Biophys. Res. Commun. 95*, 1−6.
13. Griesinger, C., Otting, G., Wüthrich, K., and Ernst, R. R. (1988) Clean-TOCSY for $^1$H spin system identification in macromolecules, *J. Am. Chem. Soc. 110*, 7870−7872.
14. Rance, M., Sorensen, O. W., Bodenhausen, G., Wagner, G., Ernst, R. R., and Wüthrich, K. (1983) Improved spectral resolution in COSY $^1$H NMR spectra of proteins via double quantum filtering, *Biochem. Biophys. Res. Commun. 117*, 479−485.
15. Bartels, C., Xia, T.-H., Billeter, M., Güntert, P., and Wüthrich, K. (1995) The program XEASY for computer-supported NMR spectral analysis of biological macromolecules, *J. Biomol. NMR 5*, 1−10.
16. Szyperski, T., Güntert, P., Otting, G., and Wüthrich, K. (1992) Determination of scalar coupling constants by inverse Fourier transformation of in-phase multiplets, *J. Magn. Reson. 99*, 552−556.
17. Linge, J. P., O'Donoghue, S. I., and Nilges, M. (2001) Automated assignment of ambiguous nuclear Overhauser effects with ARIA, *Methods Enzymol. 339*, 71−90.
18. Brünger, A. T., Adams, P. D., Clore, G. M., DeLano, W. L., Gros, P., Grosse-Kunstleve, R. W., Jiang, J. S., Kuszewski, J., Nilges, M., Pannu, N. S., Read, R. J., Rice, L. M., Simonson, T., and Warren, G. L. (1998) Crystallography and NMR system: a new software suite for macromolecular structure determination, *Acta Crystallogr., Sect. D 54*, 905−921.
19. Koradi, R., Billeter, M., and Wuthrich, K. (1996) MOLMOL: a program for display and analysis of macromolecular structures, *J. Mol. Graphics 14*, 51−55, 29−32.
20. Laskowski, R. A., Rullmannn, J. A., MacArthur, M. W., Kaptein, R., and Thornton, J. M. (1996) AQUA and PROCHECK-NMR: programs for checking the quality of protein structures solved by NMR, *J. Biomol. NMR 8*, 477−486.
21. Hutchinson, E. G., and Thornton, J. M. (1996) PROMOTIF—a program to identify and analyze structural motifs in proteins, *Protein Sci. 5*, 212−220.

22. Brickmann, J., Goetze, T., Heiden, W., Moeckel, G., Reiling, S., Vollhardt, H., and Zachmann, C.-D. (1995) Interactive visualization of molecular scenarios with MOLCAD/SYBYL, in *Data Visualization in Molecular Science—Tools for Insight and Innovation* (Bowie, J. E., Ed.) pp 83−97, Addison-Wesley Publishing Company Inc., Reading, MA.
23. Wüthrich, K. (1986) *NMR of proteins and nucleic acids*, Wiley-Interscience, New York.
24. Güntert, P., Mumenthaler, C., and Wüthrich, K. (1997) Torsion angle dynamics for NMR structure calculation with the new program DYANA, *J. Mol. Biol. 273*, 283−298.
25. Brünger, A. T. (1992) *The X-PLOR software manual (version 3.1)*, Yale University Press, New Haven, CT.
26. Nilges, M. (1993) A calculation strategy for the structure determination of symmetric dimers by $^1$H NMR, *Proteins: Struct., Funct., Genet. 17*, 297−309.
27. Boisbouvier, J., Backledge, M., Sollier, A., and Marion, D. (2000) Simultaneous determination of disulphide bridge topology and 3-D structure using ambiguous intersulphur distance restraints: possibilities and limitations, *J. Biomol. NMR 16*, 197−208.
28. Delepierre, M., Prochnicka-Chalufour, A., Boisbouvier, J., and Possani, L. D. (1999) Pi7, an orphan peptide from the scorpion *Pandinus imperator*: a $^1$H NMR analysis using a nano-NMR probe, *Biochemistry 38*, 16756−16765.
29. Norton, R. S., and Pallaghy, P. K. (1998) The cystine-knot structure of ion channel toxins and related polypeptides, *Toxicon 36*, 1573−1583.
30. Craik, D. J., Daly, N. L., and Waine, C. (2001) The cystine knot motif in toxins and implications for drug design, *Toxicon 39*, 43−60.
31. Linge, J. P., Williams, M. A., Spronk, C. A., Bonvin, A. M., and Nilges, M. (2003) Refinement of protein structures in explicit solvent, *Proteins 50*, 496−506.
32. MacArthur, M. W., and Thornton, J. M. (1993) Conformational analysis of protein structures derived from NMR data, *Proteins 17*, 232−251.
33. Heitz, A., Chiche, L., Le-Nguyen, D., and Castro, B. (1989) $^1$H 2-D NMR and distance geometry study of the folding of *Ecballium elaterium* trypsin inhibitor, a member of the squash inhibitors family, *Biochemistry 28*, 2392−2398.
34. Holak, T. A., Gondol, D., Otlewski, J., and Wilusz, T. (1989) Determination of the complete 3-D structure of the trypsin inhibitor from squash seeds in aqueous solution by nuclear magnetic resonance and a combination of distance geometry and dynamical simulated annealing, *J. Mol. Biol. 210*, 635−648.
35. Savarin, P., Guenneugues, M., Gilquin, B., Lamthanh, H., Gasparini, S., Zinn-Justin, S., and Menez, A. (1998) 3-D structure of $\kappa$-conotoxin PVIIA, a novel potassium channel-blocking toxin from cone snails, *Biochemistry 37*, 5407−5416.
36. Bernard, C., Legros, C., Ferrat, G., Bischoff, U., Marquardt, A., Pongs, O., and Darbon, H. (2000) Solution structure of HpTX2, a toxin from *Heteropoda venatoria* spider that blocks Kv4.2 potassium channel, *Protein Sci. 9*, 2059−2067.
37. Davis, J. H., Bradley, E. K., Miljanich, G. P., Nadasdi, L., Ramachandran, J., and Basus, V. J. (1993) Solution structure of $\omega$-conotoxin GVIA using 2-D NMR spectroscopy and relaxation matrix analysis, *Biochemistry 32*, 7396−7405.
38. Pallaghy, P. K., Duggan, B. M., Pennington, M. W., and Norton, R. S. (1993) 3-D structure in solution of the calcium channel blocker $\omega$-conotoxin, *J. Mol. Biol. 234*, 405−420.
39. Sevilla, P., Bruix, M., Santoro, J., Gago, F., Garcia, A. G., and Rico, M. (1993) 3-D structure of $\omega$-conotoxin GVIA determined by $^1$H NMR, *Biochem. Biophys. Res. Commun. 192*, 1238−1244.
40. Narasimhan, L., Singh, J., Humblet, C., Guruprasad, K., and Blundell, T. (1994) Snail and spider toxins share a similar tertiary structure and cystine motif, *Nat. Struct. Biol. 1*, 850−852.
41. Pallaghy, P. K., Alewood, D., Alewood, P. F., and Norton, R. S. (1997) Solution structure of robustoxin, the lethal neurotoxin from the funnel-web spider *Atrax robustus*, *FEBS Lett. 419*, 191−196.
42. Fletcher, J. I., Chapman, B. E., Mackay, J. P., Howden, M. E. H., and King, G. F. (1997) The structure of versutoxin ($\delta$-atracotoxin-Hv1) provides insights into the binding of site 3 neurotoxins to the voltage-gated sodium channel, *Structure 5*, 1525−1535.
43. Holak, T. A., Habazettl, J., Oschkinat, H., and Otlewski, J. (1991) Structures of proteins in solution derived from homonuclear 3-D NOE-NOE nuclear magnetic resonance spectroscopy. High-resolution structure of squash trypsin inhibitor, *J. Am. Chem. Soc. 113*, 3196−3198.
44. Nilges, M., Habazettl, J., Brunger, A. T., and Holak, T. A. (1991) Relaxation matrix refinement of the solution structure of squash trypsin inhibitor, *J. Mol. Biol. 219*, 499−510.
45. Gao, G. H., Liu, W., Dai, J. X., Wang, J. F., Hu, Z., Zhang, Y., and Wang, D. C. (2001) Solution structure of PAFP-S: a new knottin-type antifungal peptide from the seeds of *Phytolacca americana*, *Biochemistry 40*, 10973−10978.
46. Fujitani, N., Kawabata, S., Osaki, T., Kumaki, Y., Demura, M., Nitta, K., and Kawano, K. (2002) Structure of the antimicrobial peptide tachystatin A, *J. Biol. Chem. 277*, 23651−23657.
47. Fletcher, J. I., Dingley, A. J., Smith, R., Connor, M., Christie, M. J., and King, G. F. (1999) High-resolution solution structure of gurmarin, a sweet-taste suppressing plant polypeptide, *Eur. J. Biochem. 264*, 525−533.
48. Saether, O., Craik, D. J., Campbell, I. D., Sletten, K., Juul, J., and Norman, D. G. (1995) Elucidation of the primary and 3-D structure of the uterotonic polypeptide kalata B1, *Biochemistry 34*, 4147−4158.
49. Isaacs, N. W. (1995) Cystine knots, *Curr. Opin. Struct. Biol. 5*, 391−395.
50. Cornet, B., Bonmatin, J.-M., Hetru, C., Hoffmann, J. A., Ptak, M., and Vovelle, F. (1995) Refined 3-D solution structure of insect defensin A, *Structure 3*, 435−448.
51. Da Silva, P., Jouvensal, L., Lamberty, M., Bulet, P., Caille, A., and Vovelle, F. (2003) Solution structure of termicin, an antimicrobial peptide from the termite *Pseudacanthotermes spiniger*, *Protein Sci. 12*, 438−446.
52. Jennings, C., West, J., Waine, C., Craik, D., and Anderson, M. (2001) Biosynthesis and insecticidal properties of plant cyclotides: the cyclic knotted proteins from *Oldenlandia affinis*, *Proc. Natl. Acad. Sci. U.S.A. 98*, 10614−10619.
53. Gressent, F., Rahioui, I., and Rahbé, Y. (2003) Characterization of a high-affinity binding site for the pea albumin 1b entomotoxin in the weevil *Sitophilus*, *Eur. J. Biochem. 270*, 2429−2435.
54. Mbaiguinam, M. Détermination des causes de la résistance des légumineuses aux charançons des céréales du genre *Sitophilus*, Ph.D. Thesis, Université Claude Bernard Lyon I, 1996, pp 1−164.
55. Lu, G. (2000) TOP: a new method for protein structure comparisons and similarity searches, *J. Appl. Crystallogr. 33*, 176−183.
56. Holm, L., and Sander, C. (1993) Protein structure comparison by alignment of distance matrices, *J. Mol. Biol. 233*, 123−138.
57. Rosengren, K. J., Wilson, D., Daly, N. L., Alewood, P. F., and Craik, D. J. (2002) Solution structures of the cis- and trans-Pro30 isomers of a novel 38-residue toxin from the venom of *Hadronyche infensa* sp. that contains a cystine-knot motif within its four disulfide bonds, *Biochemistry 41*, 3294−3301.
58. Lamberty, M., Caille, A., Landon, C., Tassin-Moindrot, S., Hetru, C., Bulet, P., and Vovelle, F. (2001) Solution structures of the antifungal heliomicin and a selected variant with both antibacterial and antifungal activities, *Biochemistry 40*, 11995−12003.
59. Omecinsky, D. O., Holub, K. E., Adams, M. E., and Reily, M. D. (1996) 3-D structure analysis of $\mu$-agatoxins: further evidence for common motifs among neurotoxins with diverse ion channel specificities, *Biochemistry 35*, 2836−2844.
60. Adams, M. E., Herold, E. E., and Venema, V. J. (1989) Two classes of channel-specific toxins from funnel-web spider venom, *J. Comput. Physiol. A 164*, 333−342.
61. Pallaghy, P. K., Nielsen, K. J., Craik, D. J., and Norton, R. S. (1994) A common structural motif incorporating a cystine knot and a triple-stranded $\beta$-sheet in toxic and inhibitory polypeptides, *Protein Sci. 3*, 1833−1839.


BI034803L